



On the axisymmetric spreading of non-Newtonian power-law gravity currents of time-dependent volume: An experimental and theoretical investigation focused on the inference of rheological parameters



Sandro Longo^a, Vittorio Di Federico^{b,*}, Renata Archetti^b, Luca Chiapponi^a, Valentina Ciriello^b, Marius Ungarish^c

^a Dipartimento di Ingegneria Civile, Ambiente Territorio e Architettura (DICATeA), Università di Parma, Parma, Italy

^b Dipartimento di Ingegneria Civile, Chimica, Ambientale e dei Materiali (DICAM), Università di Bologna, Bologna, Italy

^c Dept. Computer Science, Technion, Haifa, Israel

ARTICLE INFO

Article history:

Received 4 May 2013

Received in revised form 30 July 2013

Accepted 31 July 2013

Available online 8 August 2013

Keywords:

Gravity current

Viscous

Power-law fluid

Shear thickening

Box model

Rheological parameters

ABSTRACT

We study axisymmetric gravity currents consisting of a constant or time-dependent volume of a power-law viscous fluid propagating on a horizontal rigid plane below a fluid of lesser density. The intruding fluid is considered to have a pure Ostwald–DeWaele power-law constitutive equation. First, the conditions for buoyancy–viscous balance are examined, and the current rate of spreading is derived with a box-model. An existing self-similar solution to the nonlinear differential problem for the influx of a constant or time-variable volume of fluid is then described. Results from a number of experiments conducted in a 30° sector with shear thinning, Newtonian and shear thickening fluids, and with constant and increasing release rate, are presented and interpreted with the theoretical solution, obtaining globally a very satisfactory agreement. The rheological parameters of the fluid, derived with a best fit procedure, are compared to those measured independently with conventional rheometry. Confidence intervals are evaluated for both estimates of flow behavior and consistency indices. Results support the feasibility of controlled constant flux laboratory experiments with gravity currents in axisymmetric geometry to infer the rheology of power-law fluids, especially at very low shear rates and with shear thinning fluids.

© 2013 Elsevier B.V. All rights reserved.

1. Introduction

Gravity currents are ubiquitous in many natural and artificial settings; they are essentially driven by the force of gravity acting on density differences between the fluid; this effect is also referred to as buoyancy. This buoyancy force pushes the fluid into horizontal motion, and then may be balanced mainly by inertial forces, and the current is then defined inviscid, or inertial; or by viscous forces, thereby qualifying the current as viscous.

The study of viscous and inertial gravity currents has generated a large amount of literature, including a number of books [1,2] and review papers [3–6]. Classical studies of viscous horizontal gravity currents under a lubrication approximation include Hoult [7], Didden and Maxworthy [8], and Huppert [9]. Their theoretical findings were analyzed experimentally, among others, by Huppert and Simpson [3], Maxworthy [10], and Didden and Maxworthy [8]. A stability analysis was performed by Snyder and Tait [11].

During its evolution, a current may transition from the inertial to the viscous regime (or the opposite, depending on the rate of

influx); this typically happens in several geophysical, environmental and industrial applications such as mudflows, lava flows, and mold filling.

Several fluids of interest for these applications in the viscous regime exhibit a marked non-Newtonian behavior, ranging from fluids described adequately by a simple power-law model to more complex behavior including e.g. viscoplasticity [12] and thixotropy [13].

Different approaches were employed in the literature to analyze the viscous spreading of non-Newtonian fluids over horizontal or inclined surfaces. An analytical approach solving momentum and mass balance equations via asymptotic expansions under the thin current assumption was adopted to analyze the spreading of a three-parameter Herschel–Bulkley fluid [14–18]. When a two-parameter power-law model is considered, the spreading problem is amenable to self-similar solutions: examples of this approach are found in Pascal [19], Gratton et al. [20], Balmforth et al. [14], Di Federico et al. [21], Sayag and Worster [22]. The release of a finite volume of a power-law fluid over a denser inviscid one under the influence of gravity and capillarity was analyzed by Pegler et al. [23]. These solutions typically allow a prediction of both the current rate of spreading and its profile in space–time. An alternative

* Corresponding author. Tel.: +39 0512093750; fax: +39 0516448346.

E-mail address: vittorio.difederico@unibo.it (V. Di Federico).

approach is constituted by the box model, which couples a simplified geometric representation of the current with volume continuity and balance of forces; this approach [1,2,24–27], allows capturing the current rate of spreading but not its profile. Box modeling was applied to a two-dimensional current of power-law fluid by Chowdhury and Testik [28], who compared it to an earlier self-similar solution [21], finding that the box model captures the correct dependence of the current front on time but overpredicts the position of the front, except for very shear thinning fluids.

Experimental work to validate theoretical predictions concerning gravity currents of power-law fluids was presented, among others, in [28,29,22]. In all cases validation of existing analytical formulations was limited to decidedly shear thinning fluids with low flow behavior index n . Two-dimensional experiments performed with an aqueous suspension of Kaolinite clay particles, yielded flow behavior indices in the range 0.12–0.52 for constant volume [29], and 0.15–0.33 for constant flux experiments [28]. Sayag and Worster [22] analyzed constant volume and constant flux axisymmetric spreading of aqueous suspensions of xanthan gum of 1% concentration by weight, deriving $n = 0.164$ – 0.175 (in the manuscript, Sayag and Worster use $1/n$ as fluid behavior index); in their paper, they suggested that tests performed in axisymmetric geometry under constant flux release conditions could be utilized to derive the fluid rheological properties in lieu of conventional rheometers. Such an approach has been earlier suggested by Piau and Debiane [30], who analyzed both plane (Bostwick) and axisymmetric (Adams) consistometers; in these devices an analytical solution describing the transient slumping of a constant volume of power-law fluid on a horizontal base allows estimation of fluid parameters. The use of Bostwick consistometers to infer the rheological properties of yield-stress non-Newtonian fluids, common in the food industry, was discussed by Perona [31], Milczarek and McCarthy [32], and Balmforth et al. [33].

In view of such applications, there is a need to extend the body of experiments dealing with the slumping of axisymmetric gravity currents, broadening the range of flow behavior indices examined; to our knowledge, a thorough validation of existing self-similar solutions for shear thickening fluid has never been presented in the literature. Moreover, the overall quality of predictions needs to be assessed by estimating the uncertainties associated with rheological parameters obtained with gravity current propagation, as opposed to those derived with conventional rheometers.

This paper aims at answering these open questions by further exploring the dynamics of gravity currents of power-law non-Newtonian fluids in axisymmetric geometry. To this end, Section 2 first presents a simple box model approach, capable of deriving the correct time dependence of the current rate of advancement; it then recalls an existing self-similar solution to the problem based on thin layer theory. Section 3 describes the experimental setup and methodology adopted to conduct tests with Newtonian, shear thinning, and shear thickening fluids in constant and variable flux release, illustrating: (i) predictions of rheological parameters via the theoretical model; (ii) independent rheometric measurements of fluid parameters. The two sets of estimates and their associated uncertainties are discussed and compared in Section 4. A set of conclusions (Section 5) closes the paper.

2. Theoretical results for axisymmetric viscous power-law gravity currents

We consider a horizontal, axisymmetric gravity current of an incompressible power-law non-Newtonian fluid of density ρ at the bottom of an ambient fluid of density $\rho - \Delta\rho$ (see Fig. 1).

We assume the current is changing volume in time according to $V = Qt^\alpha$ where $\alpha (\geq 0)$ and $Q (> 0)$, having dimensions $L^3 T^{-\alpha}$ are given

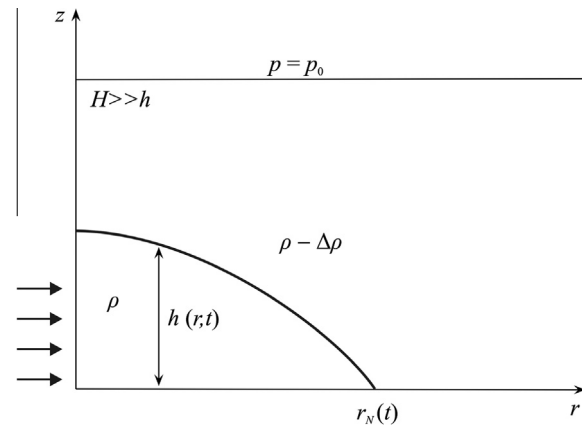


Fig. 1. Layout of the problem.

constants; note that here Qt^α is the volume per full circle, hence $Q = 2\pi q$ if the volume coefficient per radian q is given. The $\alpha = 0$ case gives the simple fixed-volume current, and the $\alpha = 1$ case corresponds to a current supplied by a constant-rate influx (say, by an open tap). The $\alpha > 1$ cases may represent a leak or eruption which worsens with time. We assume that the source is located at the center $r = 0$. In the present Section, first a simplified derivation of the position of the current head $r_N(t)$ is presented via a box model; then the self-similar solution to the problem provided in [16] is recapitulated.

2.1. Box model

The “box model” is a simple tool for the investigation of gravity currents. The approximation is of the volume-integral type: we make some simplified assumptions on the behavior of the main dependent variables (shape of the interface, dependency of the speed of the current on r , etc.), then impose volume continuity and momentum balance on the entire volume of the current. The problem is thus reduced to a set of (usually two) ODEs, whose solution is straightforward. There is a large body of evidence (see for example [2] and references therein) that this approximation provides useful results for the rate of propagation of the current, and for the transition between the inertia-buoyancy to viscous-buoyancy regimes. This motivates the use of this method in the present investigation.

The first major simplification is that the current is a cylinder of radius $r_N(t)$ and height $h_N(t)$. This is actually a similarity assumption.

The volume continuity requirement for the box model is

$$\frac{1}{2} r_N^2(t) h_N(t) = V_r = qt^\alpha, \quad (1)$$

where $h_N(t)$ is the current representative height and $V_r = V/2\pi$ the volume per radian; in the particular case $\alpha = 0$ we can replace V_r with q .

The following simplified behavior is assumed:

$$r_N = Kt^\beta, \quad h_N = \frac{2V_r}{r_N^2} = \frac{2q}{K^2} t^{\alpha-2\beta}, \quad (2)$$

$$u_N = \beta Kt^{\beta-1}, \quad u(r, t) = u_N \frac{r}{r_N} = \beta t^{-1} r, \quad (3)$$

where $u(r, t)$ is the horizontal radial velocity, u_N is the velocity of the current front, and β and K are constants to be determined by the solution.

The relevant forces can now be estimated as follows. The driving “buoyancy” force is the integral of $\partial p / \partial r$ over the volume of

the current. This effect is represented by the pressure force on the periphery “dam” which bounds the current in the box (per radian)

$$F_b = \frac{1}{2} \rho g' r_N h_N^2, \quad (4)$$

where $g' = g(\Delta\rho/\rho)$ is reduced gravity.

The inertial forces are

$$F_i = \rho h_N \int_0^{r_N} u u_r r dr = \frac{1}{3} \rho u_N^2 r_N h_N. \quad (5)$$

The power-law for the shear is of the form

$$\tau_{zr} = m \left| \frac{\partial u}{\partial z} \right|^{n-1} \frac{\partial u}{\partial z}, \quad (6)$$

with z vertical coordinate, τ_{zr} shear stress, m and n indices of fluid consistency and flow behavior; hence upon assuming $u(r, t) = u_N(r, t)(r/r_N(t))$, the viscous force at the bottom (per radian) is approximated by

$$F_v = m \int_0^{r_N} \left(\frac{u}{h_N} \right)^n r dr = \frac{1}{n+2} m \left(\frac{u_N}{h_N} \right)^n r_N^2. \quad (7)$$

We consider a current dominated by viscous reaction to the buoyancy driving (the inertial effects are negligible). Letting $F_v = F_b$ we obtain

$$u_N^n = \frac{n+2}{2m} \rho g' \frac{h_N^{n+2}}{r_N}. \quad (8)$$

We substitute the postulated forms of $h_N(t)$, $r_N(t)$, $u_N(t)$ in terms of K and β , and equate the powers of t and the coefficients. This yields

$$\beta = \frac{\alpha(n+2) + n}{3n+5}, \quad (9)$$

$$K = \beta^{-n/(3n+5)} \left[(n+2) 2^{n+1} \frac{1}{m} \rho g' q^{n+2} \right]^{1/(3n+5)}. \quad (10)$$

For $n = 1$ and $m = \mu$ the classical results of the viscous Newtonian fluid box-model are recovered, in particular $\beta = (3\alpha + 1)/8$; see Eqs. (7.21) and (7.22) of Ungarish [2].

Also of interest is the critical value of α , α_c , for which the current preserves its viscous (or inviscid) regime for all t . The box model provides this value. First we note that, according to (5) and (7),

$$\frac{F_i}{F_v} = \frac{\rho(n+2)}{3m} \frac{u_N^2 r_N h_N}{(u_N/h_N)^n r_N^2}. \quad (11)$$

Substituting the dependencies of h_N , r_N , u_N on t , we find that the ratio F_i/F_v behaves like $C_1 t^\gamma$, where

$$C_1 = \frac{(2+n)}{3m} \beta^{2-n} K^{1-n} \left(\frac{2q}{K^2} \right)^{n+1} \rho, \quad (12a, b)$$

$$\gamma = \frac{\alpha(n+3) - 2(n+5)}{3n+5},$$

and for β the result (9) was used. For $n = 1$ Eqs. (12a,b) give Eq. (7.12) in Ungarish [2]. The value $\gamma = 0$ corresponds to

$$\alpha_c = 2 \frac{n+5}{n+3}. \quad (13)$$

For $\alpha = \alpha_c$, the ratio F_i/F_v is the constant C_1 which in this case is dimensionless and can be regarded as a Reynolds number (or the inverse of a Julian number, see Maxworthy, [10]). This C_1 may be small or large, depending on the values ρ , g' , q , m , n .

For $\alpha < \alpha_c$, the ratio F_i/F_v decreases with time, and for $\alpha > \alpha_c$ this ratio increases with time; for $n = 1$ the classical result $\alpha_c = 3$ is recovered.

The solution developed here assumes that the gravity current is in the viscous–buoyancy regime, i.e., that F_i/F_v is small. The other relevant regime is the inertial–buoyancy one, i.e. F_i/F_v is large. Since the ratio F_i/F_v is, in general, a time dependent monotonic function, a gravity current is expected to change its regime of propagation. It is convenient to define the time of transition between these regimes as t_1 , when $F_i/F_v = 1$. In the present solution, we obtain

$$t_1 = (1/C_1)^{1/\gamma} \equiv \left[\frac{(2+n)}{3m} \beta^{2-n} K^{1-n} \left(\frac{2q}{K^2} \right)^{n+1} \rho \right]^{-1/\gamma}. \quad (14)$$

Concerning the realistic behavior of the gravity current, this is a quite rough estimate, because: (i) from the physical point of view, the transition from one regime to the other is not sharp; there certainly is a time interval about t_1 during which the buoyancy is counterbalanced by both inertial and viscous effects. (ii) The calculation in (14) contains the uncertainties of the box-model postulated shape and velocity r -profile. Experience shows that, in general, box models predicts accurately the value of β , but K deviates by typically 15–20% from measured values. We can expect a similar behavior in the present case.

Finally, we recall that when $\alpha = \alpha_c$ no transition takes place and therefore (14) predicts $t_1 \rightarrow \infty$ in this limit.

Our viscous–buoyancy solution is thus relevant: (i) for $t > t_1$ when $\alpha < \alpha_c$, and (ii) for $t < t_1$ when $\alpha > \alpha_c$. When $\alpha = \alpha_c$, our solution is relevant for all t , provided that C_1 is small.

We note in passing that Sayag and Worster [22] used a time dependent ‘Reynolds number’ as a counterpart to our F_i/F_v estimate (cf. (4.1) in that paper with our (11), and recall that their n is $1/n$ here). Due to a misprint in that paper, the time-decay power of that ratio seems different from our γ .

2.2. Self-similar solution

Sayag and Worster [22] (see also [34]) provide a full self-similar solution to the propagation of a viscous axisymmetric gravity current of a power-law fluid over a horizontal impermeable bottom, under the hypotheses of thin current and hydrostatic pressure.

Momentum balance and the hydrostatic hypothesis yield

$$\rho g' \frac{\partial h}{\partial r} - m n \left| \frac{\partial u}{\partial z} \right|^{n-1} \frac{\partial^2 u}{\partial z^2} = 0, \quad (15)$$

subject to the boundary conditions

$$u(z=0) = 0; \quad \frac{\partial u}{\partial z}(z=h) = 0. \quad (16)$$

Integration of (15) with (16) yields the following expression for the velocity u

$$u(z) = -\frac{n}{(n+1)} \left(\frac{\rho g'}{m} \right)^{1/n} \left| \frac{\partial h}{\partial r} \right|^{1/n-1} \times \frac{\partial h}{\partial r} h^{(n+1)/n} \left[1 - \left(1 - \frac{z}{h} \right)^{(n+1)/n} \right]. \quad (17)$$

Local and integral mass balance give respectively

$$\frac{\partial h}{\partial t} + \frac{1}{r} \frac{\partial}{\partial r} \int_0^h r u(z) dz = 0, \quad (18)$$

$$2\pi \int_0^{r_N(t)} r h(r, t) dr = Q t^\alpha, \quad (19)$$

with boundary conditions at $r = r_N$

$$h = 0, \quad \int_0^h u dz = h \frac{dr_N}{dt}. \quad (20)$$

Substituting (17) into (18) yields:

$$\frac{\partial h}{\partial t} - \frac{n}{2n+1} \left(\frac{\rho g'}{m}\right)^{1/n} \frac{1}{r} \frac{\partial}{\partial r} \left[r h^{(2n+1)/n} \left| \frac{\partial h}{\partial r} \right|^{1/n-1} \frac{\partial h}{\partial r} \right] = 0. \quad (21)$$

To solve Eqs. (19) and (21) with (20) we introduce the similarity variable

$$\xi = \left(\frac{n}{2n+1} \left(\frac{\rho g'}{m}\right)^{1/n} Q^{(n+2)/n} \right)^{-n/(3n+5)} r t^{-(\alpha(n+2)+n)/(3n+5)}, \quad (22)$$

and indicate with ξ_N the value of ξ for $r = r_N$.

Then the similarity solution is of the form

$$h(r, t) = \xi_N^{(n+1)/(n+2)} Q \left[\frac{n}{2n+1} \left(\frac{\rho g'}{m}\right)^{1/n} Q^{(n+2)/n} \right]^{-2n/(3n+5)} t^{(\alpha(n+1)-2n)/(3n+5)} \Psi(\chi), \quad (23)$$

with $\chi = \xi/\xi_N$.

Substituting (22) and (23) in (19)–(21) yields

$$\begin{aligned} \frac{d}{d\chi} \left[\chi \Psi^{2(n+1)/n} \left| \frac{d\Psi}{d\chi} \right|^{1/n-1} \frac{d\Psi}{d\chi} \right] \\ + \frac{\alpha(n+2)+n}{3n+5} \chi^2 \frac{d\Psi}{d\chi} - \frac{\alpha(n+1)-2n}{3n+5} \chi \Psi = 0, \end{aligned} \quad (24)$$

$$\Psi = 0; \quad \Psi^{2(n+1)/n} \left| \frac{d\Psi}{d\chi} \right|^{1/n-1} \frac{d\Psi}{d\chi} = 0 \quad \text{for } \chi = 1, \quad (25)$$

$$\xi_N(\alpha, n) = \left(2\pi \int_0^1 \chi \Psi d\chi \right)^{-(n+2)/(3n+5)}. \quad (26)$$

Once ξ_N is determined, the position of the current front is given by

$$r_N(t) \equiv R = \xi_N \left[\frac{n}{2n+1} \left(\frac{\rho g'}{m}\right)^{1/n} Q^{(n+2)/n} \right]^{n/(3n+5)} t^{(\alpha(n+2)+n)/(3n+5)}. \quad (27)$$

Upon comparing expression (27) with that derived by the box model, it is noted that the box model provides the correct power of t , and the correct parametric dependency of the coefficient, but differs in the numerical value of the latter. Fig. 2 depicts the ratio between the current extension estimated with the box model and with the similarity solution; it is seen that the box model tends to overestimate the current leading edge by a factor increasing with n and slightly increasing with α . The overestimation is about 20% for the Newtonian flow, as earlier observed [2]. This is so since the box model assumes a horizontal interface, while the exact

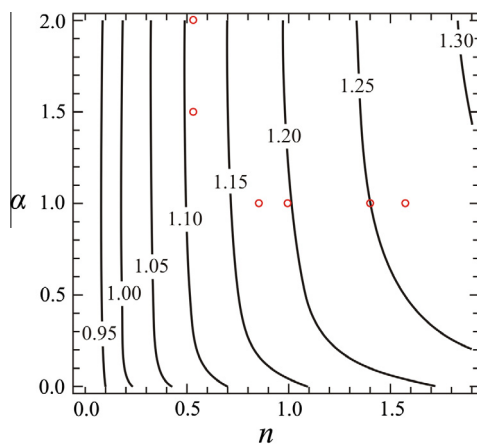


Fig. 2. Ratio between current spread-out estimated with the box model and exact analytical solution. Circles indicate some experimental points of the present dataset.

solution has a forward-inclined interface. Therefore, near the nose, the exact solution predicts a larger shear hindrance than the box model, and hence a smaller rate of spread-out. It is however observed that for very shear thinning fluids with rheological index below a threshold value (decreasing with increasing α), the box model underestimates the propagation distance. This tendency was already observed by Chowdhury and Testik [28] in plane geometry, with the threshold value being approximately equal to $n = 0.25$; here, due to the different geometry, the threshold is around $n = 0.20$ and nearly independent from α . A possible explanation of this inversion in behavior is as follows. The box model flat h_N actually reduces the buoyancy force F_b . In a real current, the height over which the pressure pushes is larger than the averaged h_N , and hence the real F_b is larger than the prediction (4). When n is not small, this reduction of F_b is more than counterbalanced by the reduction of the shear imposed by the constant h_N of the box model. However, when n is small, the shear is less sensitive to the thickness, and therefore the box model underpredicts the real propagation.

Eq. (24) is solved numerically for any value of $\alpha > 0$ using, as a starting condition for integration, the asymptotic analytical solution near $\chi = 1$ in the form of a Frobenius series

$$\begin{aligned} \Psi(\chi) = a_0 (1 - \chi)^{n+2} \\ \left[1 + (1 - \chi) \frac{n \left[(15 + 14n + 3n^2) + a_0^{-n+2} (2+n)^{\frac{1}{2}} [n(\alpha-6) + n^2(\alpha-2) - 2\alpha] \right]}{(3+n) \left[(20 + 27n + 9n^2) - (2+n)^{\frac{1}{2}} a_0^{-3} n(n+2\alpha+n\alpha) \right]} \right], \\ a_0 = (n+2)^{\frac{1}{n+2}} \left[\frac{\alpha(n+2)+n}{3n+5} \right]^{\frac{n}{n+2}}, \end{aligned} \quad (28)$$

generalizing the expression (2.27) given for a Newtonian fluid in Huppert [9], after correcting an error or typo. The correct expression for $n = 1$ is

$$\Psi(\chi) = \left[\frac{3}{8} (3\alpha + 1) \right]^{\frac{1}{3}} (1 - \chi)^{\frac{1}{3}} \left[1 - \frac{1 - 3\alpha}{6(3\alpha + 1)} (1 - \chi) + O(1 - \chi)^2 \right]. \quad (29)$$

In the case $\alpha = 0$ the problem is amenable to an analytical solution,

$$\Psi(\chi) = \left(\frac{n}{3n+5} \right)^{n/(n+2)} \left(\frac{n+2}{n+1} \right)^{1/(n+2)} (1 - \chi^{n+1})^{1/(n+2)}, \quad (30)$$

$$\xi_N = \left\{ \frac{2\pi}{3n+5} \left(\frac{n}{3n+5} \right)^{n/(n+2)} \left(\frac{n+2}{n+1} \right)^{1/(n+2)} \frac{\Gamma[2/(n+1)] \Gamma[1/(n+2)]}{\Gamma[(3n+5)/(n+1)(n+2)]} \right\}^{-(n+2)/(3n+5)}. \quad (31)$$

3. Experiments

A thorough validation of the similarity solution is important in view of the possible use of axisymmetric gravity current to determine rheological properties of complex fluids in lieu of, or in parallel to, conventional rheometers. A comparison between the theoretical prediction of the front position and experimental results has been already carried out for Newtonian fluids [8,9,35] in plane and axisymmetric geometry, and for shear thinning fluids in air [22], but data on the behavior of currents of shear thickening fluids are scarce. This is so not only because shear thinning behavior is the most common deviation from Newton's law, but also because, while shear thinning fluids are relatively easy to prepare and handle, most known shear thickening fluids are suspensions subject to sedimentation and rapid variations of their rheological properties. In addition, all available experiments with power-law fluids refer to a constant-volume ($\alpha = 0$) or constant-flux ($\alpha = 1$) release. A relevant set of experiments for Newtonian currents with

variable inflow rate and 2D geometry is reported in [10]; no such tests are available for non-Newtonian fluids.

In the following the results from four sets of experiments aimed at validating the similarity solution are reported. The first set of experiments was conducted with shear thickening fluids and constant inflow rate ($\alpha = 1.0$); the second set included experiments with shear thinning fluids with constant and increasing inflow rate ($\alpha = 1.0, 1.5, 2.0$). A third set of experiments with Newtonian fluids was performed to validate the overall procedure and set-up. Finally, tests in critical inflow rate conditions were performed for Newtonian and shear thinning fluids. All the fluids used in the experiments were subject to an independent measurement of the apparent viscosity via conventional rheometers, in order to compare the rheological parameters thus derived with those yielded by the gravity current measurements.

3.1. Rheometry

Shear thinning fluids used in controlled laboratory experiments are often obtained adding organic additives to water or other Newtonian fluids. Amongst the additives, carboxymethyl cellulose (CMC) and xanthan gum are widely used because they are not expensive and give stable mixtures with predictable rheological characteristics (see [36]). Their rheological behavior is fully described by a Cross or Carreau–Yasuda model, and reduces to the Ostwald–DeWaele power-law model for intermediate ranges of shear rates. For the present tests, a mixture of glycerol, water and CMC (2% in weight) or xanthan gum (0.1% in weight) was prepared and tested with a parallel plate rheometer (Dynamic Shear Rheometer Anton Paar Physica MCR 101).

As a shear thickening fluid, a suspension of cornstarch in water was prepared at a concentration of 100 wt.%. This corresponds to a volume fraction of $\phi = 32.3\%$ assuming a density of 1550 kg/m^3 [37]. The rheological behavior of the mixture was tested with a classical coaxial cylinders shear rheometer (Haake Rotovisco

RT10), as the parallel plate rheometer could not be used due to the tendency of cornstarch to sediment. The rheometric results showed an evident dilatancy behavior except at very low shear rates, where shear thinning behavior was recorded. A similar mixture was analyzed in [38] with an extensional rheometer, showing a behavior analogous to that observed in the present tests.

Fig. 3 shows the measured apparent viscosity as a function of shear rate for four mixtures used in the present experiments: two cornstarch suspensions in panels (a and c), a mixture of glycerol, water and CMC or xanthan gum in (b and d) respectively. It is evident that power-law behavior constitutes a local approximation of the constitutive equation since the regression of the experimental data indicates different values of the coefficient and of the exponent for different intervals of measured data. Hence the correct interval of shear rate to be considered in the derivation of rheological parameters depends on the shear rate experienced by the tested gravity currents. As easily derived from the analytical solution described earlier, the magnitude of the shear rates for most of the current body (excluding zones near the origin and the front end) is less than 2 or 3 s^{-1} . For this reason the fluid rheological and consistency indices m and n were inferred from measurements in the lower interval of shear rates (blue crosses). In this range, the thin dashed lines indicate the prediction interval at the 95% of confidence level (we assumed that the uncertainty is equal to the root mean square of the residual between rheometric data and the rheological power-law model). Note that the spatial variability in shear rate experienced by the current during its propagation (in the vertical and radial directions) adds further dispersion to experimental values of m and n inferred from the experiments.

3.2. Experimental setup

The experiments took place at the Hydraulics Laboratory of the University of Parma. A 30° sector of a flat PVC surface limited by PVC walls was chosen to mimic a fully axisymmetric current since

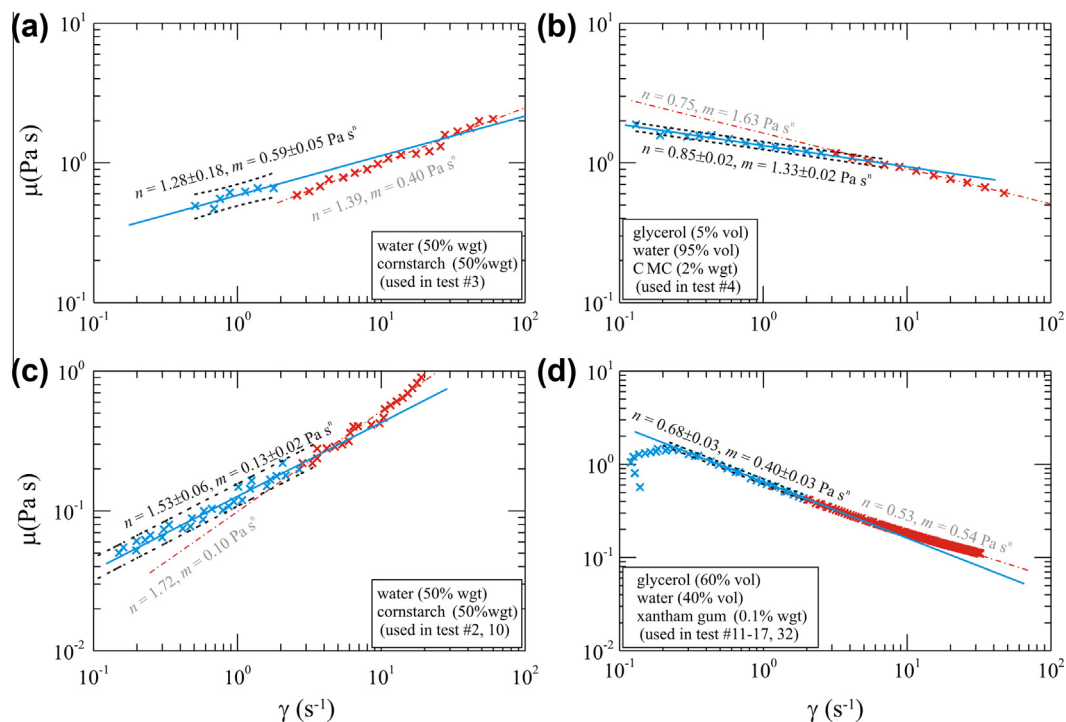


Fig. 3. Rheometric tests for different fluids used in the experiments. The bold blue lines indicate the least square regression for the low shear rate range, the dash-dot red lines indicate the least square regression for the high shear rate range. The dashed curves represent the prediction limit at 95% of confidence level in the low shear rate range. (For interpretation of the references to color in this figure legend, the reader is referred to the web version of this article.)

the maximum pump discharge was not sufficient to reach the selected values of the flux. This configuration enhances the resistance encountered by the current, since a boundary layer develops also along the vertical walls limiting the circular sector. However, since the thickness of the current is very small as compared to the lateral width, the surface of contact with the vertical wall is a small fraction of that with the base, except for the early spreading stage when inertia dominates the whole process anyway. The support of the horizontal surface is in PVC and leveled through three adjustable feet; an electronic spirit level (Digital Protractor 82201B-00), with an overall accuracy equal to $1/10^\circ$, granted the horizontality of the plane of spreading. Two different syringe pumps were employed: the first, built up in the laboratory, has three 60 ml plastic syringes in parallel, and a piston moved by a DC motor and positioned through an Ultrasonic distance meter sensor. A gear reduction allows a large variation of the flux, reaching a maximum value of 3.9 ml/s with a relative accuracy 1%. This pump was used for most tests performed with constant flux ($\alpha = 1$), including those with the cornstarch suspension having shear thickening behavior. In this case, several devices were needed since the cornstarch grains tend to settle out fairly quickly, altering the rheological behavior of the mixture. To minimize this phenomenon, the syringe pump was directly connected to the injection hole through a short pipe, and the experiment started immediately after the refilling of the syringe. The second pump employed is a commercial Teledyne ISCO 260D Syringe Pump, with a maximum capacity of 266 ml, a flow accuracy of 0.5% of the set point and a maximum flux of 1.78 ml/s. This pump can be controlled by a PC with DAQ software in order to generate time increasing flux. The ISCO pump was used to perform one of the experiments with constant flux and all experiments with variable (increasing) flux. Note that these tests were performed only with a shear thinning fluid, since the shear thickening cornstarch and water mixture could not be filled in the cylinder of the pump and could not flow into the connecting pipe because of its small radius (1 mm internal diameter).

The current spreading was recorded by a high resolution video camera (1920×1080 pixels) working at 25 frames/s and with a resolution better than $6 \text{ pixel} \cdot \text{mm}^{-1}$ in the experimental conditions of the present tests. A non-linear transformation of the single frames allowed to obtain a plane undistorted image, with the transformation parameters computed recording a single shot of a reference grid containing at least four points of known coordinates in the current plane. Several algorithms were employed in sequence to detect the boundary of the current front and transfer each frame to data files. If glares of light were absent in the captured images, as in experiments with cornstarch suspensions, a software for automatic detection of the front of the gravity current was quite effective and allowed the automatic analysis of all frames (25 frames/s) and the extraction of the coordinates of the leading edge. In other tests, glares of light were present in the images, and a semi-automatic detection of the front was performed extracting 2 frames/s. Since the detection of the advancing current boundary is based on a gray level transformation with a fixed threshold, considering the resolution of the video camera used results in a point measurement uncertainty of 0.5 mm. For each time step, the current radius r_N was taken to be the average of the local coordinate of the leading edge over the entire 30° sector (except 5 mm near the walls).

The setup is shown in Fig. 4 and the whole set of experiments performed is listed in Table 1, which reports: the pump flow rate; the type of test (constant or variable influx); the fluid used and its rheology; the fluid density measured with the laboratory scale; the values of the rheological parameters n and m measured directly by rheometric tests (r) and estimated by analyzing experimental data measured during the viscous spreading of constant flux gravity

currents (gc), as detailed in Section 3.3; the difference between the two estimates.

3.3. Analysis of constant flux experiments

In this subsection we describe the constant flux experiments (conducted with a full circle discharge ranging between 14.7 and 16.0 ml s^{-1}) and discuss how they are used to derive the fluid rheological parameters via regression analysis, and the extent of associated uncertainties. If the experimental apparatus is used as a rheometer, the raw output data is the front end position as a function of time; with the acquisition protocol discussed in Section 3.2, the front end position at each time is a spatial average over the circle sector. The model used to interpret the experimental data is represented in the most general case by Eq. (27), which can be expressed in compact form as $r_N(t) = f(n, m, \rho, g', Q, t, \alpha)$. Assuming further that the mass density ρ , the volumetric discharge Q and the reduced gravity g' are exempt from errors, the model parameters reduce to n and m . The regression analysis is performed with a grid search method, (i) allowing the two parameters n and m to vary in a given interval, (ii) computing the theoretical value of r_N as a function of time, (iii) finding the values of the parameters that minimize a measure of the error between theoretical model and experimental data (the residuals); this measure is assumed herein equal to the sum of the squares of the differences between the experimental and computed front end position. To evaluate the uncertainty associated with the estimate of rheological parameters, we note that the sources of uncertainties lie in the measures of time, t , and of the current front, r_N , and in the goodness of the model itself in reproducing the physical phenomenon. The measurement error associated with time is extremely small (of the order of the shutter speed, $1/500 \text{ s}$ in the present experiments) and decidedly negligible. The measurement error associated with the current spread, if r_N is evaluated as an average value along the arc of advancement, is due to the camera resolution, to the lenses and to the algorithm of detection of the boundary. Providing a high camera resolution, adequate lenses and a smart algorithm, this error is also quite small, of the order of 0.5 mm in the present tests as earlier specified; note however that if the current spread is measured along a single radius (e.g. using a laser sheet with a range finder as in [22]), then the potential variability of the front end position along the arc needs to be taken into account (the spatial variability of the front end position, assumed equal to the sample standard deviation, is reported in Fig. 5 for two of the present experiments).

In general measurement uncertainties in t and r_N can be safely neglected since the associated error is very low in absolute value and also compared to the uncertainty in the model, which is dominant.

In practice, Eq. (27) is monomial and can be reduced to a linear one by taking the logarithms of both sides. Then we assume that the error is equal to the root mean square of the residual between experimental data and the model. The usual rules for propagating the variances (see, e.g., Bevington and Robinson [39]) allow the evaluation of the variance of m and n and the computation of the 95% confidence limits reported in Table 1 for the rheological parameters deduced from the constant flux experiments.

Fig. 5a and b shows an example of the regression analysis conducted for a shear thinning (test #4) and a shear thickening fluid (test #10). The upper panel in Fig. 5a and b shows the optimal model regression (solid line) of experimental data, where the fitting parameters are the flow behavior and consistency indices n and m . The best-fit procedure is performed only on a subset of experimental points fulfilling the thin layer approximation, which is considered satisfied if the average ratio $h/r_N \approx Qt^2/\pi r_N^3 < 0.1$. In our experiments, the h/r_N ratio decreases with time, and the

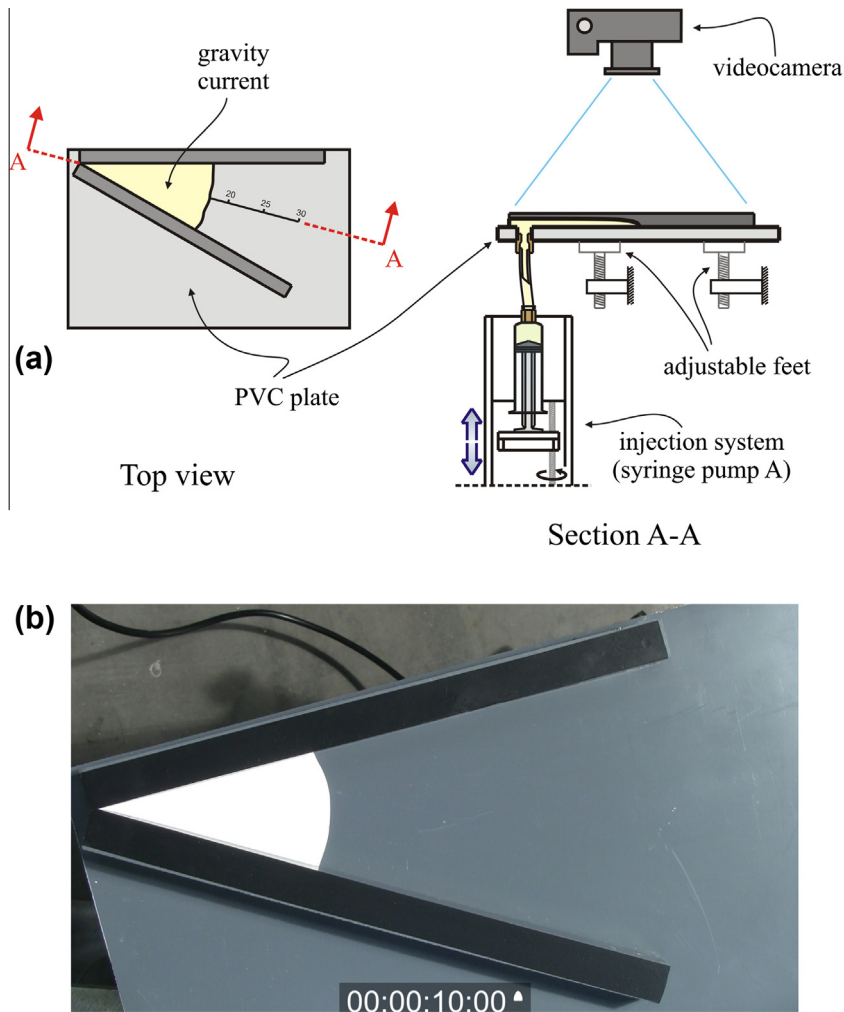


Fig. 4. (a) The experimental apparatus used for release with constant and time-increasing flux. (b) Snapshot of constant-flux experiment with shear thickening fluid, test #10 (top view).

Table 1

Set of experiments. The ambient fluid is air. ρ is the mass density of the current fluid, m and n are the consistency index and the fluid behavior index estimated through rheometers (r), or through gravity current measurements (gc). The carrier fluid was water for cornstarch, glycerol and water for CMC and xanthan gum. A tiny quantity of ink was added to increase the contrast between the current and the bottom wall. The 95% confidence limits are shown in parameters estimates. Bold characters indicate that the estimates are statistically different, since their difference does not include zero.

Test #	Full circle flow rate Q (ml s ⁻¹)	α (.)	Fluid (rheology)	ρ (kg m ⁻³)	m (r) (Pa s ⁿ)	n (r) (.)	m (gc) (Pa s ⁿ)	n (gc) (.)	$m(r) - m(gc)$ (Pa s ⁿ)	$n(r) - n(gc)$ (.)
2	16.0	1.0	cornstarch (shear thickening)	1200	0.13 ± 0.02	1.53 ± 0.06	0.18 ± 0.13	1.66 ± 0.06	-0.05 ± 0.14	-0.13 ± 0.09
3	14.7	1.0	cornstarch (shear thickening)	1200	0.59 ± 0.05	1.28 ± 0.18	0.55 ± 0.47	1.20 ± 0.08	0.04 ± 0.48	0.08 ± 0.16
4	15.0	1.0	CMC (shear thinning)	1022	1.33 ± 0.02	0.85 ± 0.02	1.50 ± 0.71	0.85 ± 0.04	-0.17 ± 0.72	0.00 ± 0.05
8	21.4	1.0	glycerol (Newtonian)	1259	0.54 ± 0.04	1.0 ± 0.02	0.89 ± 0.44	1.02 ± 0.06	-0.35 ± 0.44	-0.02 ± 0.06
10 [*]	15.1	1.0	cornstarch (shear thickening)	1200	0.13 ± 0.02	1.53 ± 0.06	0.18 ± 0.02	1.50 ± 0.02	-0.05 ± 0.03	0.03 ± 0.06
11	3.0√ t	1.5	xanthan gum (shear thinning)	1159	0.40 ± 0.03	0.68 ± 0.03				
12 [*]	0.24 t	2.0	xanthan gum (shear thinning)	1159	0.40 ± 0.03	0.68 ± 0.03				
14	3.72 × 10 ⁻⁴ $t^{2.5}$	3.5	xanthan gum (shear thinning)	1159	0.40 ± 0.03	0.68 ± 0.03				
15	4.80 × 10 ⁻⁵ $t^{3.0}$	4.0	xanthan gum (shear thinning)	1159	0.40 ± 0.03	0.68 ± 0.03				
16	1.88 × 10 ⁻³ $t^{2.13}$	3.13	xanthan gum (shear thinning)	1159	0.40 ± 0.03	0.68 ± 0.03				
17	1.80 × 10 ⁻³ $t^{2.0}$	3.0	xanthan gum (shear thinning)	1159	0.40 ± 0.03	0.68 ± 0.03				
18	1.80 × 10 ⁻³ $t^{2.0}$	3.0	glycerol, water (Newtonian)	1239	0.21 ± 0.04	1.0 ± 0.04				
19	3.60 × 10 ⁻³ $t^{2.0}$	3.0	glycerol, water (Newtonian)	1239	0.21 ± 0.04	1.0 ± 0.04				
23	18.0 × 10 ⁻³ $t^{2.0}$	3.0	glycerol, water (Newtonian)	1239	0.21 ± 0.04	1.0 ± 0.04				
32	13.15 × 10 ⁻³ $t^{2.13}$	3.13	xanthan gum (shear thinning)	1159	0.40 ± 0.03	0.68 ± 0.03				

* It indicates the tests where video is available as supplementary material, <http://dx.doi.org/10.1016/j.jnnfm.2013.07>.

position where that criterion becomes valid is represented in the graphs by the dotted vertical line. A second characteristic time of the spreading phenomenon, represented by the vertical dash-dotted line in the upper panel of Fig. 5a and b, is determined by the

balance between inertial and viscous forces. The ratio between these forces is of $O(1)$ at the time t_1 given by the box model's Eq. (14). It is noted that for constant flux experiments: (i) the current transitions to the viscous regime before the thin layer

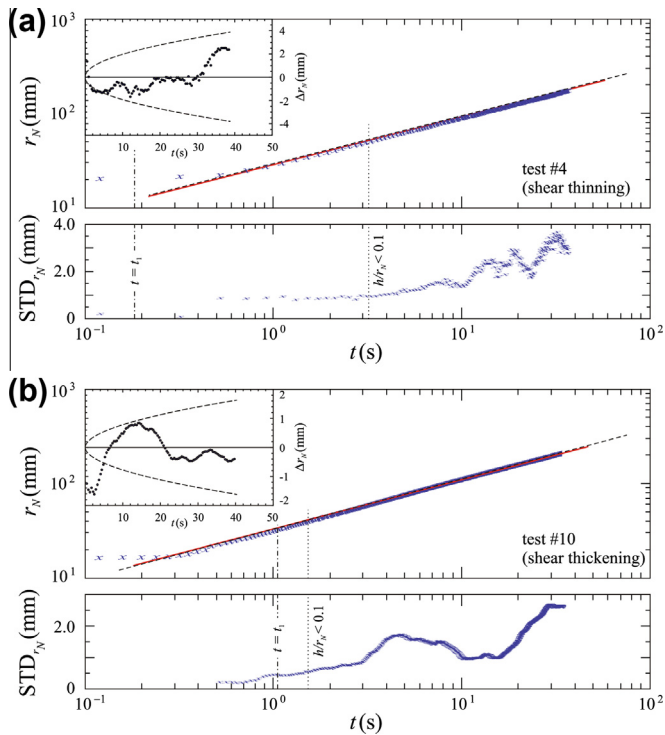


Fig. 5. (a) Upper panel: position of the average of the leading edges over the 30° sector for a constant flux gravity current of a shear thinning fluid (test # 4) versus time. Symbols represent experimental data, the solid line represents the optimal fitting of the theoretical model including only data in the thin-layer approximation regime. The dashed line represents the model results with the values of m and n as given by rheometric tests (sixth and seventh column in Table 1). The insert indicates the difference between the measured r_N and the model value of r_N (symbols) derived by optimal fitting, and the prediction interval at 95% of confidence level (dashed lines). Lower panel: standard deviation of the leading edges over the 30° sector versus time. The dash-dotted line marks the transition to the viscous–buoyancy regime, the dotted line marks the transition to the thin layer approximation regime. (b) Same as (a) except for a shear thickening fluid (test # 10).

approximation is valid; (ii) the theoretical model, derived under the thin layer approximation, interprets experimental results well for a mean gradient much larger than $1/10$, and can be considered to hold even in a time range where inertia dominates, on the left side of the dash-dotted line.

Fig. 5a and b also include (dashed straight line) the theoretical curve corresponding to the values of n and m derived independently from the rheometrical tests. It is noted that a good agreement is found with experimental points, and the result is hardly distinguished from the solid line representing the best fit; for the remaining constant flux tests the agreement is still good.

The insert in the upper panel of Fig. 5a and b shows the aforementioned difference Δr_N between the measured front position and its model value calculated using the best-fitting rheological parameters, and the corresponding prediction interval at 95% confidence level.

Finally, the lower panel in Fig. 5a and b depicts the spatial standard deviation STD of the front position over the 30° sector as a function of time; this quantity is seen to increase on average with time, albeit not monotonously, attaining maximum values of 2–4 mm for total test durations of approximately 40 s. In fact, upon observing the current spreading (see video #1 depicting test #10 in Supplementary material) it is noted that the leading edge of the current is not a perfect arc but exhibits several lobes continuously appearing and disappearing, and advances with a sinuous shape characterized by a limited standard deviation. Similar phenomena were observed for laminar gravity currents intruding into a viscous miscible ambient fluid [11] and were attributed to: (i) gravity,

when the nose of the current is elevated above the bottom surface because of its irregularities and overrides a layer of ambient fluid buoyantly unstable and (ii) viscous fingering akin to Saffman–Taylor instability and occurring if the ambient fluid is more viscous than the intruding fluid. The currents of the present tests are always much more viscous than the ambient fluid (air), hence only buoyancy instability could be advocated; however, a series of photographs of the current nose with macrolens did not reveal any nose elevation of the advancing current above the bottom, hence instability due to gravity could not develop. In addition, the lobes become less evident for faster currents, obtained upon increasing the pump discharge. We are thus inclined to attribute the sinuosity of the leading edge to heterogeneity in local conditions (cleanliness and roughness) of the bottom surface, which modify the contact angle and induce variability of the radial position of the current edge. Fast advancing currents are less sensible to this effect and thus exhibit lesser spatial variations in the position of the current leading edge, as confirmed by the smaller values of STD obtained for the shear thickening current of test #10 than for the shear thinning current of test #4.

3.4. Analysis of variable flux experiments in subcritical influx regime

In this subsection we succinctly describe the experiments conducted with increasing flux in subcritical regime with the Teledyne ISCO 260D pump in order to simulate the conditions $\alpha = 1.5, 2.0$ and 3.0 (tests #11, 12 and 17); all tests were performed with a shear thinning fluid, as visible in video #2 showing test #12, which is included in Supplementary material. Fig. 6 shows for two of these tests (#11 and #12) the experimental results as a function of time, the threshold of validity of the thin layer approximation (dotted lines), and the time of transition t_1 to the viscous–buoyancy regime. It is noted that while both currents enter the thin layer approximation regime after a short time (2–5 s), inertia forces are dominant with respect to buoyancy forces in test #12, for which the current reaches the balance at $t_1 \approx 26$ s. Nevertheless, the analytical solution (27) was juxtaposed to experimental data using the values of rheological parameters deduced from the rheometric tests (solid lines in Fig. 6). In test #12 it is evident that a transition between regimes of propagation occurred during the recorded motion. It is noted that the overall fitting for test #12 is relatively good, despite the fact that most experimental data lie outside the domain of validity of the model.

3.5. Overview of test results

Fig. 7 shows experimental results in dimensionless form for the subcritical tests with $\alpha < \alpha_c$; length and time scales are given respectively by $h^* = Q^{n/(3n+\alpha)}(m/(\rho g'))^{2/(3n+\alpha)}$, $t^* = (m/(\rho g' h^*))^{1/n}$. In

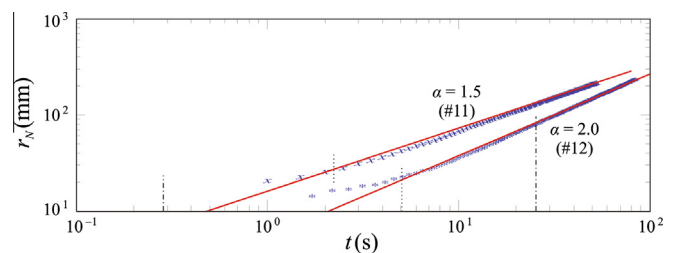


Fig. 6. Experimental results for a variable flux release (tests #11 and #12) of a shear thinning mixture of glycerol (60% in volume), water (40% in volume) and xanthan gum (0.1% in weight) plus ink. The solid line represents the theoretical model (27) valid in viscous–buoyancy regime with consistency and flow behavior indices obtained by rheometric measurements. Shear thinning fluid $n = 0.68 \pm 0.01$, $m = 0.40 \pm 0.01$ Pa sⁿ. The dotted lines mark the transition to the thin layer approximation regime, the dash-dotted line marks the transition to the viscous–buoyancy regime.

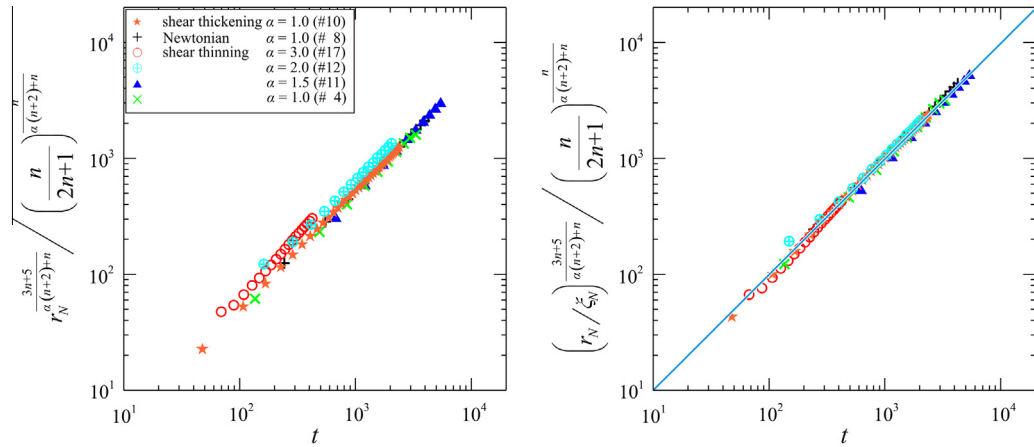


Fig. 7. Experimental results for tests in subcritical conditions. Left panel: experimental data without coefficient; right panel: experimental data scaled with the coefficient ζ_N evaluated through the numerical model. Parameters n and m are those obtained through a best fitting procedure if applicable (i.e. if the thin-layer approximation and the viscous–buoyancy regime hold), otherwise the values measured with rheometer listed in Table 1 are used. The straight line indicates a perfect agreement. For better visualization the number of experimental points is reduced to 1/5.

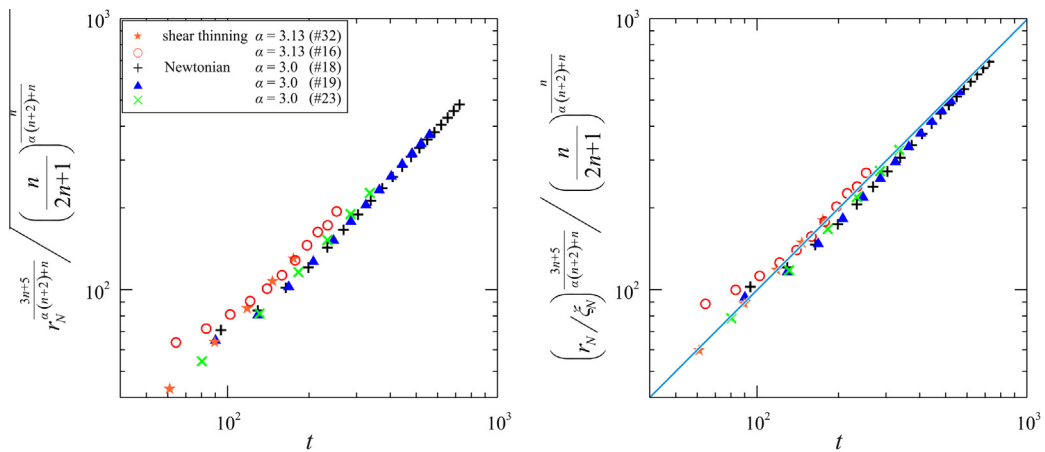


Fig. 8. Same as Fig. 7 except tests in critical conditions.

the left panel the inclination of the fitting lines should be 1:1 but a vertical offset is expected since the dimensionless coefficient ζ_N is not included. The right panel shows the same data including also ζ_N evaluated through numerical integration of (26). The data collapse fairly well with minor deviations from the perfect agreement at early times. Fig. 8 is similar to Fig. 7, except that it shows experimental results in critical conditions (not discussed in detail earlier); in this case the collapsing is worse than in Fig. 7, but still acceptable.

Globally the theoretical solution demonstrated a very satisfactory agreement with experimental investigations conducted in subcritical and critical conditions.

4. Discussion

In this section a comparison is drawn between rheological parameters derived with conventional rheometers and gravity currents with constant flux. Preliminarily, we observe that upon juxtaposing to the experimental data of all tests (see Fig. 5 for tests #4 and #10) the theoretical model (27) with the adoption of the values of n and m measured with the rheometers, a good agreement was found (dashed line).

Best fitting of experimental results for CMC (test #4) revealed shear thinning behavior with $n = 0.85 \pm 0.04$, $m = 1.50 \pm 0.71 \text{ Pa}\cdot\text{s}^n$.

The parallel-plate rheometer yielded for the same mixture $n = 0.85 \pm 0.02$, $m = 1.33 \pm 0.02 \text{ Pa}\cdot\text{s}^n$ at a temperature $T = 22.5 \text{ }^\circ\text{C}$. The flow behavior index computed by curve fitting is coincident with the results of the strain-controlled rheometer, and the associated uncertainty is very low for both methods; the two values derived for the consistency index differ to some extent, with the value deriving from the gravity current being higher by 12.7%, and having a much larger associated uncertainty; the difference in the values of n and m estimated with the two methods is $n(r) - n(gc) = \pm 0.05$ and $m(r) - m(gc) = -0.17 \pm 0.72$ with a 95% confidence level; since zero is included in the interval for both parameters we conclude that there is no statistically significant difference in the two methods for estimating n and m .

A similar behavior is observed for a Newtonian fluid (test #8), where both rheometers reconstitute unity for the fluid behavior index, but the gravity current yields a larger viscosity than the rheometer.

The three tests conducted with cornstarch suspension (#2, #3, and #10) yielded shear thickening behavior in all cases, albeit with differences between tests, to be attributed to the specific nature of the suspension which tends to be unstable and to sediment, rendering the experimental conditions more difficult to reproduce.

For Test #2 the parameters deduced by means of the best fitting procedure ($n = 1.66 \pm 0.06$, $m = 0.18 \pm 0.13 \text{ Pa}\cdot\text{s}^n$) differ quite significantly from those obtained with the coaxial-cylinders rheometer, which yielded for the same mixture $n = 1.53 \pm 0.06$,

$m = 0.13 \pm 0.02 \text{ Pa s}^n$ at a temperature $T = 21.9 \text{ }^\circ\text{C}$. It results $n(r) - n(\text{gc}) = -0.13 \pm 0.09$ and $m(r) - m(\text{gc}) = -0.05 \pm 0.14$; hence the 95% confidence limits for the estimate of flow behavior index do not include zero, while those relative to the consistency index do. The statistical difference is significant.

Results of Test #10 are somewhat similar to those obtained for Test #2, in that rheological parameters and associated confidence limits derived by means of conventional rheometer are identical to Test #2, while the parameters deduced via gravity current are $n = 1.50 \pm 0.02$ and $m = 0.18 \pm 0.02$; the former result is in excellent agreement with that obtained with the strain-controlled rheometer, while the consistency index differs significantly (38.5% higher) and is statistically different at 95% confidence level (see Table 1).

Two factors combine to bring about this effect. The first one is that best fitting of the rheometric experimental data (shear rate vs shear stress) at low values of shear rate for shear thickening fluids reduces the flow behavior index and increases the consistency index (for shear thinning fluids it generally increases both parameters, see [22]), and shear stresses in experimental conditions are on average moderately lower than those usually detected in the rheometric tests. The second factor is the time and space variability of the rheology of the cornstarch mixture during current spreading; this phenomenon is likely due to sedimentation of cornstarch grains (which was observed at the end of our tests), producing heterogeneity along the vertical.

Finally, the rheological behavior of the mixture was decidedly different for Test #3, which yielded $n = 1.20 \pm 0.08$, $m = 0.55 \pm 0.47 \text{ Pa s}^n$ as best fit parameters, to be compared with $n = 1.28 \pm 0.18$, $m = 0.59 \pm 0.05 \text{ Pa s}^n$ measured at a temperature $T = 22.7 \text{ }^\circ\text{C}$ with the conventional rheometer. The rheological parameters obtained with the two methods are in statistically significant agreement, even though the confidence interval associated with the gravity current measurement of the consistency index is larger.

On a final note, in the previous analysis it was assumed that the temperature of the fluid is homogeneous and time-invariant and also not significantly different from the temperature of the fluid during rheometric tests. In general a further source of uncertainty arises if these hypotheses are violated.

5. Conclusions

The following conclusions may be derived from our theoretical and experimental study of horizontal axisymmetric spreading of non-Newtonian power-law gravity currents:

1. A simplified expression for the speed of propagation and nose position was derived via a box-model and compared with that obtained from lubrication theory. Both approaches yield propagation with t at the same power, but there is some difference in the coefficient. The deviation between predictions calculated with the two models depends on fluid flow behavior index and type of release; the box model overpredicts the spreading rate except for very shear thinning fluids with $n < 0.20$. The box model also yields an estimate of the relevant forces acting on the current and of the transition time between the inertial and the viscous regime. It is concluded that the proposed box-model solution can provide a fairly accurate description of the viscous spreading of power-law gravity currents, usable for quick estimations. We must keep in mind, however, that this approximation lacks rigor, and its applicability outside the range of parameters tested in this study cannot be assessed.
2. A previously-published analytical solution for gravity currents in viscous buoyancy regime was validated with constant flux experiments conducted with shear thinning, Newtonian, and shear thickening fluids; these allowed to derive the rheological

parameters of the fluid with a best fit procedure. Globally a very good agreement was found between experimental and analytical results, as demonstrated by: (i) the collapse of experimental data for tests in subcritical conditions onto a single curve expressing the theoretical solution in dimensionless form and (ii) the inclusion of model estimates of the front end of the current in the corresponding prediction interval at 95% confidence level. However, we must keep in mind that the analytical results are valid only when (1) the thickness ratio h/r_N is small (< 0.1 , say) and (2) the flow is in the viscous–buoyancy domain. For $\alpha < \alpha_c$, this is not satisfied in the initial stage, and hence the good agreements can be observed only in the later stage of a sufficiently long experiment.

3. The rheological parameters of all fluids used in the experiments were measured independently with conventional rheometrical tests, allowing a comparison between the two sets of parameters.
4. A key point in the assessment of the goodness of the estimate of rheological parameters via conventional rheometers or gravity current propagation is the estimation of the associated error. This was estimated for both sets of parameters in the form of 95% confidence limits.
5. The comparison between values of rheological parameters derived upon calibrating the analytical solution against experimental results and those derived via direct rheological measures yields results depending on the nature of the fluid, and valid within the range of parameters tested in this study. For shear thinning and Newtonian fluids, the two estimates of flow behavior index coincide and exhibit a very low associated error, while the consistency index derived by current propagation is higher than that of the conventional rheometer, and has a larger associated uncertainty; the difference in the estimates of the parameters with the gravity current device and with classical rheometers are statistically not significant at 95% confidence level for all tests except Test #2 and Test #10, both with shear thickening fluids. The difference in consistency index is linked to the variability of the mean shear rate in current propagation with respect to the range of shear rate used to approximate with a power-law the shear-stress shear-rate diagrams obtained with the rheometers. For shear thickening fluids, the flow behavior and consistency indices estimated with the gravity current may be lower or higher than that of the rheometer; the error associated with flow behavior index is generally quite low for both estimates, while that linked to consistency index may be significantly higher, as already noted for the shear thinning fluid. Results obtained for shear thickening fluid are influenced by the specific nature of cornstarch suspensions used in the experiments, as grains in the mixture tend to settle out, altering the rheological behavior of the mixture and inducing its spatial variability.
6. Our experiments confirm that axisymmetric gravity currents are a viable alternative to conventional rheometry for the determination of rheological parameters of power-law fluids. The different fluid nature has implications towards the practical feasibility of the idea of using constant flux experiments as a rheometer. While shear thinning fluids similar to those adopted in our experiments exhibit only spatial variability of the shear rate, suspensions with shear thickening behavior display also spatial variability in their composition connected to possible particle sedimentation, evident in their two-layer structure. Hence for shear thinning fluids constant flux experiments can be used in lieu of rheometers to determine fluid parameters; this is especially convenient at very low shear rates, since shear-controlled rheometers, even the most sophisticated and accurate, fail to obtain a correct response at very low shear rates due to mechanical friction. For shear thickening fluids, on one

hand the spurious effects described may limit the use of gravity currents as rheometers. On the other hand, the use of gravity current may prove useful to estimate the rheological parameters for shear thickening mixtures including grains of relevant size, not easily accommodated in a conventional rheometer.

7. Our work demonstrates the advantage of the wedge geometry: reliable results were obtained with a significantly smaller amount of fluid and pump discharge than necessary for similar experiments with full-circle currents.

Acknowledgments

MU acknowledges the hospitality of the Centre for Geophysical Flows, School of Mathematics, University of Bristol, UK, where a part of this research was performed.

Appendix A. Supplementary material

Supplementary data associated with this article can be found, in the online version, at <http://dx.doi.org/10.1016/j.jnnfm.2013.07.008>.

References

- [1] J.E. Simpson, Gravity Currents: In The Environment and The Laboratory, second ed., Cambridge University Press, Cambridge, 1997.
- [2] M. Ungarish, An Introduction to Gravity Currents and Intrusions, CRC Press, Boca Raton, 2009.
- [3] H.E. Huppert, J.E. Simpson, The slumping of gravity currents, *J. Fluid Mech.* 99 (1980) 785–799.
- [4] J.E. Simpson, Gravity currents in the laboratory, atmosphere, and ocean, *Ann. Rev. Fluid Mech.* 14 (1982) 213–234.
- [5] H.E. Huppert, The intrusion of fluid mechanics into geology, *J. Fluid Mech.* 173 (1986) 557–594.
- [6] H.E. Huppert, Gravity currents: a personal perspective, *J. Fluid Mech.* 554 (2006) 299–322.
- [7] D.P. Hault, Oil spreading on the sea, *Ann. Rev. Fluid Mech.* 4 (1972) 341–368.
- [8] N. Didden, T. Maxworthy, The viscous spreading of plane and axisymmetric gravity currents, *J. Fluid Mech.* 121 (1982) 27–42.
- [9] H.E. Huppert, The propagation of two-dimensional and axisymmetric viscous gravity currents over a rigid horizontal surface, *J. Fluid Mech.* 121 (1982) 43–58.
- [10] T. Maxworthy, Gravity currents with variable inflow, *J. Fluid Mech.* 128 (1983) 247–257.
- [11] D. Snyder, S. Tait, A flow-front instability in viscous gravity currents, *J. Fluid Mech.* 369 (1998) 1–21.
- [12] G. Chambon, D. Ghemmour Laigle, Gravity-driven surges of a viscoplastic fluid: an experimental study, *J. Non-Newton. Fluid Mech.* 158 (2009) 54–62.
- [13] H. Chanson, S. Jarny, P. Coussot, Dam break wave of thixotropic fluid, *J. Hydraul. Eng. ASCE* 132 (2006) 280–293.
- [14] N.J. Balmforth, A.S. Burbidge, R.V. Craster, J. Salzig, A. Shen, Visco-plastic models of isothermal lava domes, *J. Fluid Mech.* 403 (2000) 37–65.
- [15] N.J. Balmforth, R.V. Craster, A.C. Rust, R. Sassi, Viscoplastic flow over an inclined surface, *J. Non-Newtonian Fluid Mech.* 142 (2007) 219–243.
- [16] N. Dubash, N.J. Balmforth, A.C. Slim, S. Cochar, What is the final shape of a viscoplastic slump?, *J. Non-Newton. Fluid Mech.* 158 (2009) 91–100.
- [17] A.J. Hogg, G.P. Matson, Slumps of viscoplastic fluids on slopes, *J. Non-Newton. Fluid Mech.* 158 (2009) 101–112.
- [18] C. Ancey, S. Cochar, The dam-break problem for Herschel–Bulkley viscoplastic fluids down steep flumes, *J. Non-Newton. Fluid Mech.* 158 (2009) 18–35.
- [19] J.P. Pascal, Gravity flow of a non-Newtonian fluid sheet on an inclined plane, *Int. J. Eng. Sci.* 29 (10) (1991) 1307–1313.
- [20] J. Gratton, F. Minotti, S.M. Mahajan, Theory of creeping gravity currents of a non-Newtonian liquid, *Phys. Rev. E* 60 (6) (1999) 6960–6967.
- [21] V. Di Federico, S. Malavasi, S. Cintoli, Viscous spreading of non-Newtonian gravity currents on a plane, *Meccanica* 41 (2006) 207–217.
- [22] R. Sayag, M.G. Worster, Axisymmetric gravity currents of power-law fluids over a rigid horizontal surface, *J. Fluid Mech.* 716 (R5) (2013) 1–11.
- [23] S. Pegler, J.R. Lister, M.G. Worster, Release of a viscous power-law fluid over an inviscid ocean, *J. Fluid Mech.* 700 (2012) 63–76.
- [24] M.A. Hallworth, A.J. Hogg, H.E. Huppert, Effects of external flow on compositional and particle gravity currents, *J. Fluid Mech.* 359 (1998) 109–142.
- [25] C. Gladstone, A.W. Woods, On the application of box models to particle-driven gravity currents, *J. Fluid Mech.* 416 (416) (2000) 187–195.
- [26] A.J. Hogg, M. Ungarish, H.E. Huppert, Particle-driven gravity currents: asymptotic and box model solutions, *Eur. J. Mech. B – Fluids* 19 (2000) 139–165.
- [27] T. Harris, A.J. Hogg, H.E. Huppert, Polydisperse particle-driven gravity currents, *J. Fluid Mech.* 472 (2002) 333–371.
- [28] M.R. Chowdhury, F.Y. Testik, Viscous propagation of two-dimensional non-Newtonian gravity currents, *Fluid Dyn. Res.* 44 (2012) 045502, <http://dx.doi.org/10.1088/0169-5983/44/4/045502>.
- [29] M.R. Chowdhury, F.Y. Testik, Laboratory testing of mathematical models for high-concentration fluid mud turbidity currents, *Ocean Eng.* 38 (2011) 256–270.
- [30] M.P. Piau, K. Debiante, Consistometers rheometry of power-law viscous fluids, *J. Non-Newton. Fluid Mech.* 127 (2005) 213–224.
- [31] P. Perona, Viscoplastic dam breaks and the Bostwick consistometer, *Appl. Rheol.* 15 (4) (2005) 218–219.
- [32] R. Milczarek, K.L. McCarthy, Relationship between the Bostwick measurement and fluid properties, *J. Text. Stud.* 37 (6) (2006) 640–654.
- [33] N.J. Balmforth, R.V. Craster, P. Perona, A.C. Rust, R. Sassi, Viscoplastic dam breaks and the Bostwick consistometer, *J. Non-Newtonian Fluid Mech.* 142 (2007) 63–78.
- [34] V. Di Federico, S. Malavasi, Propagazione di una corrente di densità non newtoniana in geometria radiale (in Italian), in: *Atti del XXIX Convegno di Idraulica e Costruzioni Idrauliche*, Trento, 7–10 settembre 2004, vol. 1, 2004, pp. 117–124.
- [35] R.E. Britter, J.E. Simpson, Experiments on the dynamics of a gravity current head, *J. Fluid Mech.* 88 (1978) 223–240.
- [36] M.P. Escudier, I.W. Gouldson, A.S. Pereira, F.T. Pinho, R.J. Poole, On the reproducibility of the rheology of shear thinning liquids, *J. Non-Newton. Fluid Mech.* 98 (2001) 99–124.
- [37] J. Yang, A. Sliva, A. Banerjee, R.N. Dave, R. Pfeffe, Dry particle coating for improving the flowability of cohesive powders, *Powd. Technol.* 158 (2005) 21–33.
- [38] E.E. Bischoff White, M. Chellamuthu, J.P. Rothstein, Extensional rheology of a shear-thickening cornstarch and water suspension, *Rheol. Acta* 49 (2009) 119–129.
- [39] P.R. Bevington, D.K. Robinson, *Data Reduction and Error Analysis*, McGraw-Hill, New York, 2003.